

# Signatures of inhomogeneous dark matter annihilation on 21-cm

Junsong Cang<sup>1,\*</sup>, Yu Gao<sup>2,†</sup> and Yin-Zhe Ma<sup>4,5,‡</sup>

<sup>1</sup> *School of Physics, Henan Normal University, Xinxiang, China*

<sup>2</sup> *Key Laboratory of Particle Astrophysics, Institute of High Energy Physics, Chinese Academy of Sciences, Beijing, 100049, China*

<sup>4</sup> *Department of Physics, Stellenbosch University, Matieland 7602, South Africa and*

<sup>5</sup> *National Institute for Theoretical and Computational Sciences (NITheCS), Stellenbosch University, Matieland 7602, South Africa*

The energy released from dark matter annihilation leads to additional ionization and heating of the intergalactic gas and thereby impact the hydrogen 21-cm signal during the cosmic dawn. The dark matter annihilation rate scales as density-squared and it becomes inhomogeneously boosted along with structure formation. This paper examines the inhomogeneity in DM annihilation rate induced by the growth of DM halo structures, and we show that this effect can significantly enhance the spatial fluctuations in gas temperature, gas ionization fraction and consequently the 21-cm brightness temperature. Compared to previous homogeneous calculations, inhomogeneous dark matter annihilation can enhance the 21-cm power spectrum by orders of magnitude across the scales of  $k \in [0.05, 3] \text{ Mpc}^{-1}$ . For a DM annihilation rate of  $\langle\sigma v\rangle/m_\chi \sim 10^{-27} \text{ cm}^3 \text{ s}^{-1} \text{ GeV}^{-1}$ , the corresponding signatures in the 21-cm power spectrum signal can be detected by upcoming radio observatories such as the SKA.

## I. INTRODUCTION

The annihilation events of dark matter (DM) can produce secondary particles that can potentially be detected through astrophysical probes [1, 2]. Cascades of these secondary particles can lead to extra ionization and heating of the intergalactic medium (IGM). The ionization effect enhances the scatters between the cosmic microwave background (CMB) photon on free electrons and photons, leading to observable effects in the CMB anisotropy measurements [3–8]. The latest observation of *Planck* [3] yielded DM annihilation constraints that are competitive to those from high-energy cosmic ray searches [1, 2, 9–11]. The heating effect from DM annihilation, on the other hand, can be efficiently probed by 21-cm signal from neutral hydrogen.

The 21-cm signal arises from the transition between the neutral hydrogen’s singlet and triplet states, which offers an invaluable glimpse into the cosmic dark ages and the Epoch of Reionization (EoR) [12]. During these epochs the formation of DM halo structures is expected to significantly enhance DM annihilation rate. The 21-cm signal strength is sensitive to the thermal and ionization conditions in the IGM, thereby providing a unique avenue to detect the possible heating and ionization induced by DM annihilation. The primary 21-cm observation window below redshift 20 lies deep in the nonlinear structure growth epoch, during which spatial inhomogeneity is expected to be present in the DM halo-boosted heating and ionizing sources. This can in turn lead to an enhancement in the 21-cm power spectrum at scales where the spatial inhomogeneity manifests itself.

In this paper, we examine the effects of inhomogeneity in DM distribution on 21-cm power spectrum. Our results show that the formation of DM halo structures induces inhomogeneity in DM annihilation rate that closely traces density fluctuations. Assuming that DM annihilation products have a short absorption length, which is generally feasible for relatively light-dark matter and the resultant radiation is at low energy, we find that the DM-induced heating and ionization exhibit distinctive inhomogeneous structures, which further enhances spatial fluctuation and power spectrum for 21-cm signal. Such features can be particularly helpful for discrimination of possible DM signatures from complex astrophysical background. For an annihilation rate of  $\langle\sigma v\rangle/m_\chi \sim 10^{-27} \text{ cm}^3 \text{ s}^{-1} \text{ GeV}^{-1}$ , which is roughly the same level as that constrained by cosmic ray and CMB [1–3, 9], the corresponding 21-cm power spectrum can be easily detected by the Square Kilometer Array (SKA) telescope [13].

This paper is organized as follows: Sec. II briefly reviews the basics of cosmic 21-cm signal, in Sec. III we describe our model for inhomogeneous DM annihilation, the 21-cm power spectrum results are presented in Sec. IV and we conclude in Sec. V.

## II. COSMIC 21-CM SIGNAL

The hydrogen 21-cm signal arises from the hyperfine energy split between singlet and triplet states of neutral hydrogen. In cosmological context, the strength of this signal is measured by 21-cm brightness temperature  $T_{21}$  [12, 14],

$$T_{21} \simeq 27x_{\text{HI}}(1 + \delta_b) \left( \frac{H}{dv_r/dr + H} \right) \left( 1 - \frac{T_\gamma}{T_s} \right) \times \left( \frac{1+z}{10} \frac{0.15}{\Omega_m h^2} \right)^{1/2} \left( \frac{\Omega_b h^2}{0.023} \right) \text{ mK}, \quad (1)$$

\* cangjunsong@outlook.com

† gaoyu@ihep.ac.cn

‡ mayinzhe@sun.ac.za

where  $z$  is redshift,  $x_{\text{HI}}$  is the neutral fraction of the IGM,  $\delta_b$  is baryon density contrast,  $H(z)$  is the Hubble parameter,  $dv_r/dr$  is velocity gradient along the line of sight,  $T_\gamma$  indicates the temperature of the radiation background, which is commonly assumed to be CMB temperature.  $\Omega_m$  and  $\Omega_b$  are fractional densities for matter and baryon respectively (therefore fractional density of cold dark matter is  $\Omega_c = \Omega_m - \Omega_b$ ),  $h$  is the Hubble constant in the unit of 100 km/s/Mpc. The spin temperature  $T_s$  quantifies the number density ratio of hydrogen atoms in singlet and triplet states and is coupled to both radiation temperature  $T_\gamma$  and gas kinetic temperature  $T_k$  through collisional coupling and Wouthuysen-Field effect [14, 15]

$$T_s^{-1} = \frac{T_\gamma^{-1} + x_\alpha T_\alpha^{-1} + x_c T_k^{-1}}{1 + x_\alpha + x_c}, \quad (2)$$

where the color temperature  $T_\alpha$  is closely coupled to  $T_k$ ,  $x_\alpha$  and  $x_c$  are coefficients for collisional and Wouthuysen-Field coupling (see Ref. [12]).

As can be seen from Eq. (1), spatial fluctuations of ionization, density, gas temperature and velocity gradient means that  $T_{21}$  is inherently inhomogeneous, therefore in addition to the global average  $\bar{T}_{21}$ , 21-cm signal is also characterized by its power spectrum, which is generally defined as follows,

$$\Delta_\phi^2(k, z) \equiv \frac{k^3}{2\pi^2} P_\phi(k, z), \quad (3)$$

$$\langle \tilde{\phi}(\vec{k}, z) \tilde{\phi}^*(\vec{k}', z) \rangle \equiv (2\pi)^3 \delta_D^{(3)}(\vec{k} - \vec{k}') P_\phi(k, z), \quad (4)$$

where  $\phi$  denotes the physical quantity under consideration, which can take values of  $T_{21}$ , density field  $\delta$  and boost factor  $B$  (see next section) in the context of this work. The brackets  $\langle \rangle$  denotes the ensemble average,  $\tilde{\phi}(\vec{k}, z)$  refers to the Fourier transform of  $\phi(\vec{x}, z)$ ,  $\delta_D$  is the three-dimensional Dirac function, and  $k = |\vec{k}|$ . We compute all power spectrum in our analysis using the `powerbox` package [16].

Equations (1, 2) show that 21-cm signal is encoded with information about the thermal and ionization states of IGM ( $T_k$ ,  $x_{\text{HI}}$ ). For the epochs of interests ( $5 \lesssim z \lesssim 40$ ), IGM is affected by energy injection from annihilating DM as well as the radiation from the first galaxies, therefore discrimination of possible DM signal using  $T_{21}$  requires thorough knowledge about the astrophysical background. Our calculations are built primarily on the `21cmFAST` code [14, 17], which is a fast semi-analytic package for simulating both the density field and astrophysical radiation.

Throughout this work, we adopt a  $\Lambda$ CDM cosmology with *Planck* 2018 parameters [3]. For the background astrophysics, we adopt the default `21cmFAST` setting, which has been detailly presented in Ref. [17]. Note that these setting has been shown to be consistent with measurements of UV luminosity function [18–20], optical depth [21] and reionization timing [22]. For numerical processes, we make use of the `21cmFAST` framework, and

interested readers can refer to [14, 17] for review and program details.

### III. INHOMOGENEOUS DARK MATTER ANNIHILATION

Assuming that DM particles  $\chi$  annihilate through  $s$ -wave with a thermally averaged cross-section  $\langle \sigma v \rangle$ , the energy injected per unit volume and time (referred to as injection rate hereafter for convenience) can be written as

$$\left[ \frac{dE}{dV dt} \right] = 2m_\chi \cdot g \langle \sigma v \rangle n_\chi^2 = \frac{\langle \sigma v \rangle}{m_\chi} \rho_c^2, \quad (5)$$

where  $m_\chi$  denotes DM mass,  $\rho_c$  is DM density,  $n_\chi = \rho_c/m_\chi$  is the number density of DM particle, and  $\langle \sigma v \rangle n_\chi^2$  is the number of DM annihilation events per unit volume and time,  $g$  is a symmetry factor which we take 1/2 following [3]. For homogeneous distribution, using  $\rho_c = \bar{\rho}_c = \Omega_c \rho_{\text{cr}} (1+z)^3$ , where  $\rho_{\text{cr}}$  is current critical density, Eq. (5) can be expressed as,

$$\left[ \frac{dE}{dV dt} \right]_{\text{HMG}} = \frac{\langle \sigma v \rangle}{m_\chi} \Omega_c^2 \rho_{\text{cr}}^2 (1+z)^6, \quad (6)$$

where the subscript HMG denotes homogeneous distribution.

As can be seen from Eq. (5), the global injection rate of DM is proportional to  $\rho_c^2$ , which is simply  $\bar{\rho}_c^2 = \Omega_c^2 \rho_{\text{cr}}^2 (1+z)^6$  for homogeneous distribution. As matter overdensity grows at lower redshifts ( $z \leq 50$ ), the homogeneity assumption in Eq. (6) is no longer valid, and  $\rho_c^2$  can be enhanced above  $\bar{\rho}_c^2$  by orders of magnitude. As the result, the overall DM injection rate can also be significantly enhanced. Therefore at low redshifts we model DM injection by combining the contribution from both collapsed halos and that from un-collapsed regions.

#### A. Collapsed Halos

The net annihilation rate density for DM in collapsed halos can be obtained by summing up the contribution from individual halos. The bolometric luminosity  $L_{\text{DM}}$  from DM annihilating inside a halo can be calculated by integrating Eq. (5) within the halo volume,

$$L_{\text{DM}} = \frac{4\pi \langle \sigma v \rangle}{m_\chi} \int dr r^2 \rho_c^2(r), \quad (7)$$

where  $r$  is the distance to the halo center.  $\rho_c(r)$  is radial DM density of the halo, for which we adopt the Navarro-Frenk-White (NFW) profile [23, 24],

$$\rho_c(r) = \frac{\rho_{\text{cr}}(z) \delta_c r_{\text{vir}}}{cr(1 + cr/r_{\text{vir}})^2}, \quad (8)$$

where  $\rho_{\text{cr}}(z) \equiv 3H^2/(8\pi G)$  is the critical density at redshift  $z$ ,  $G$  is the gravitational constant, and  $r_{\text{vir}}$  is the virial radius [23, 25]

$$r_{\text{vir}} = 0.784 \left( \frac{m}{10^8 h^{-1} m_{\odot}} \right)^{1/3} \left( \frac{\Omega_{\text{m}}}{\Omega_{\text{m}}^z} \frac{\Delta_{\text{c}}}{18\pi^2} \right)^{-1/3} \times \left( \frac{10}{1+z} \right) h^{-1} \text{kpc}, \quad (9)$$

where  $\Delta_{\text{c}}$  is the mean overdensity of halo relative to  $\rho_{\text{cr}}(z)$  and is given by  $\Delta_{\text{c}} = 18\pi^2 + 82d - 39d^2$ , with  $d = \Omega_{\text{m}}^z - 1$  and  $\Omega_{\text{m}}^z = \Omega_{\text{m}}(1+z)^3/(\Omega_{\text{m}}(1+z)^3 + \Omega_{\Lambda})$ ,  $\Omega_{\Lambda}$  is the fractional density parameter for dark energy.  $\delta_{\text{c}}$  is related to  $\Delta_{\text{c}}$  as,

$$\delta_{\text{c}} = \frac{\Delta_{\text{c}}}{3} \frac{c^3}{\ln(1+c) - c/(1+c)}, \quad (10)$$

where we adopt the halo concentration parameter as [23],

$$c = \frac{176.6}{1+z} \left( \frac{m}{m_{\odot}} \right)^{0.098}. \quad (11)$$

For each simulation cell, the injection rate from DM annihilating in halos is given by,

$$\begin{aligned} \left[ \frac{dE}{dVdt} \right]_{\text{Halo}} &= (1+z)^3 \int_{m_{\text{min}}} dm \frac{dn}{dm}(\delta) \cdot L_{\text{DM}} \\ &= \frac{4\pi \langle \sigma v \rangle (1+z)^3}{m_{\chi}} \\ &\times \int_{m_{\text{min}}} dm \frac{dn}{dm}(\delta) \left[ \int dr r^2 \rho_{\text{c}}^2 \right], \end{aligned} \quad (12)$$

while deriving the second line we have used Eq. (7), the prefactor of  $(1+z)^3$  converts injection rate from comoving frame to physical frame,  $\delta(x)$  is the density contrast at the cell's location,  $dn/dm(\delta)$  is the Press-Schechter conditional halo mass function computed with 21cmFAST, which describes the comoving halo number density per mass interval for a region with overdensity  $\delta$  [26–28].  $m_{\text{min}}$  is the minimum mass below which free-streaming prevents the formation of DM halos. Following Refs. [8], we adopt  $m_{\text{min}} = 10^{-6} m_{\odot}$ , which is the canonical value for WIMP (Weakly Interacting Massive Particles) dark matter.

## B. Uncollapse IGM regions

Outside the collapsed halos, we compute the DM density  $\rho_{\text{c}}$  as,

$$\rho_{\text{c}}(x) = (1 - f_{\text{coll}}) \bar{\rho}_{\text{c}}, \quad (13)$$

where  $f_{\text{coll}}$  is the fraction of matter collapsed into halos and can be computed from conditional halo mass function as,

$$f_{\text{coll}}(x) = \frac{1}{\Omega_{\text{m}} \rho_{\text{cr}}(1+\delta)} \int_{m_{\text{min}}} dm \cdot m \frac{dn}{dm}(\delta). \quad (14)$$

Inserting Eq. (13) into Eq. (5), we can obtain the injection rate from DM annihilating in uncollapsed IGM regions,

$$\left[ \frac{dE}{dVdt} \right]_{\text{IGM}} = \frac{\langle \sigma v \rangle}{m_{\chi}} [1 - f_{\text{coll}}(x)]^2 \Omega_{\text{c}}^2 \rho_{\text{cr}}^2 (1+z)^6. \quad (15)$$

## C. Inhomogeneous Boost Factor

At low redshifts the net DM injection rate is the sum of DM annihilating in halos and in uncollapsed IGM, and we parameterize the enhancement relative to injection in the uniform frame using the boost factor  $B(x)$  as defined below,

$$B(x) \equiv \left( \left[ \frac{dE}{dVdt} \right]_{\text{Halo}} + \left[ \frac{dE}{dVdt} \right]_{\text{IGM}} \right) / \left[ \frac{dE}{dVdt} \right]_{\text{HMG}} \quad (16)$$

from which the accurate injection rate can be recovered as,

$$\left[ \frac{dE}{dVdt} \right](x) = B(x) \left[ \frac{dE}{dVdt} \right]_{\text{HMG}}. \quad (17)$$

Using Eqs. (6,12) and Eq. (15) <sup>1</sup>,

$$\begin{aligned} B(x) &= [1 - f_{\text{coll}}(x)]^2 + \frac{4\pi}{\Omega_{\text{c}}^2 \rho_{\text{cr}}^2 (1+z)^3} \\ &\times \int_{m_{\text{min}}} dm \frac{dn}{dm}(\delta) \left[ \int dr r^2 \rho_{\text{c}}^2 \right]. \end{aligned} \quad (19)$$

Note that the boost factor in cosmological context has been studied in the literature (see [29, 30], etc.), and here in Eq. (19) we use the conditional halo mass function, which encodes information about density fluctuation and therefore allows us to derive inhomogeneous DM injection rate and its impact on 21-cm power spectrum. Our comprehensive treatment of the *inhomogeneous boost factor* represents the main modeling improvement in this work.

## D. Recombination equations

The energy injected from annihilating DM can in general be absorbed by the IGM and cause additional ionization and heating. The corresponding recombination equations now become [8, 31],

$$\frac{dx_{\text{e}}}{dt}(x) = \left[ \frac{dx_{\text{e}}}{dt} \right]_{\text{Fiducial}} + \frac{f_{\text{ion,DM}}}{n_{\text{H}} E_{\text{i}}} \left[ \frac{dE}{dVdt} \right](x), \quad (20)$$

<sup>1</sup> For the NFW profile, the integration for halo density profile can be solved analytically as

$$\int dr r^2 \rho_{\text{c}}^2 = \frac{\rho_{\text{cr}}^2(z) \delta_{\text{c}}^2 r_{\text{vir}}^3}{3c^3(1+c)^3} [(1+c)^3 - 1]. \quad (18)$$

$$\frac{dT_k}{dt}(x) = \left[ \frac{dT_k}{dt} \right]_{\text{Fiducial}} + \frac{2f_{\text{heat,DM}}}{3k_B n_b} \left[ \frac{dE}{dV dt} \right](x), \quad (21)$$

where the subscript “Fiducial” indicates the background evolution in absence of DM injection, which has been detailed in Refs. [14, 17].  $n_H = (1 + \delta)\bar{n}_H$  is the number density of hydrogen nuclei,  $\bar{n}_H = 0.19(1+z)^3/\text{m}^3$  is the background value of  $n_H$  assuming a helium mass fraction of  $Y_{\text{He}} = 0.245$  [3], and  $E_i = 13.6\text{eV}$  is the ionization energy of a ground-state hydrogen.

The deposition efficiencies  $f_{\text{ion,DM}}$  and  $f_{\text{heat,DM}}$  in Eqs. (20) and (21) describe the fraction of DM injection rate that goes into ionization and heating respectively. A systematic derivation of  $f_{\text{ion,DM}}$  and  $f_{\text{heat,DM}}$  can be performed by tracking the electromagnetic cascades of DM annihilation products in IGM, which depends on species and primary energy of DM annihilation product, as well as the IGM ionization and thermal states, redshifts of injection and deposition, etc. For an uniform background, such analysis was performed in Refs. [5–7, 32, 33]. Most recently Ref. [34] studied energy deposition in inhomogeneous background for DM decay. However, tracking particle cascade in an inhomogeneous universe for annihilation process is beyond the scope of this paper. While the energy injection rate for decaying DM is directly proportional to simulation cell density [34], for annihilation process the inhomogeneous energy injections are contributed almost entirely by DM inside halos, therefore for annihilating DM such analysis will likely involve scales down to halo size, which is well below the simulation cell size. The problem becomes even more complicated when taking into account the feedback from IGM, i.e. DM changes IGM environment, which in turn changes  $f_{\text{ion,DM}}$  and  $f_{\text{heat,DM}}$  and thereby DM deposition itself.

For convenience, here we model  $f_{\text{ion,DM}}$  and  $f_{\text{heat,DM}}$  with the analytic SSCK (Shull, van Steenberg, Chen & Kamionkowski) parametrization [35, 36]

$$f_{\text{ion,DM}} = \frac{1 - x_e(x)}{3}, \quad (22)$$

$$f_{\text{heat,DM}} = \frac{1 + 2x_e(x)}{3}, \quad (23)$$

which have been supported by recent simulations [7, 37–40]. Eqs. (22,23) nicely capture the IGM feedback and inhomogeneity in IGM environment, as well as the intuitive expectation that highly ionized IGM would be harder to ionize. We divide our calculation of Eqs. (20) and (21) into two stages: at high redshifts ( $z > 60$ ), we solve the recombination history by our modified HyRec package [41, 42]. As this is well before the Stelliferous Era, we ignore stellar radiation in Eqs. (20, 21) during this epoch. In the lower redshift stage ( $z \leq 60$ ), we perform the full simulation using the initial conditions for  $x_e$  and  $T_k$  set by high-redshift evolution.

## IV. SIMULATION RESULTS

We consider the following 3 different simulation settings,

- **Inhomogeneous Boost (IHM):** Our main simulation assumes inhomogeneous injection boost factor detailed in Sec. III and the background astrophysics described in Sec. II. We set DM annihilation rate to  $\langle\sigma v\rangle/m_\chi = 10^{-27}\text{cm}^3\text{s}^{-1}\text{GeV}^{-1}$ , which roughly corresponds to the current CMB constraints from *Planck* [3]. This gives a reionization optical depth of  $\tau_{\text{rei}} = 0.073$  which is also in agreement with *Planck* [3, 43].
- **Homogeneous Boost (HMG):** Similar to IHM case but instead of the inhomogeneous boost factor, we use its global average value  $\bar{B}$ . Note that all global quantities in this simulation are identical to that in IHM scenario.
- **Fiducial:** Simulation for the fiducial astrophysical background detailed in Sec. II in absence of DM injection ( $\langle\sigma v\rangle/m_\chi = 0$ ).

All our simulations are performed with  $300^3$  resolution and a box length of 500 comoving Mpc. Note that if DM annihilation products have a long mean free path before absorption, the heating and ionization rates will remain widely dispersed despite the inhomogeneity in injection rate. The HMG simulation can be seen as a representation of this scenario, and to a large extent aligns with the situation in previous analyses in [8, 29, 30, 44–49]. In contrast, as represented by the IHM simulation, if the annihilation products have a short absorption length, which is typically the case if they are injected below electroweak energy scales or if they consist mainly of electrons [5, 7, 32], the injected energy will be deposited locally, and the corresponding ionization and heating rates would be inhomogeneous.

Fig. 1 shows the inhomogeneous lightcone evolution for the boost factor, density contrast and various observables ( $x_e$ ,  $T_k$  and  $T_{21}$ ) along with comparisons between IHM and HMG simulations. From the upper 2 panels, it can be seen that the boost factor  $B$  exhibits distinctive inhomogeneity patterns that closely traces that in density contrast  $\delta$ . This is further demonstrated quantitatively in the middle and right panels of Fig. 2, where we show that after normalization,  $B$  and  $\delta$  shares remarkably similar power spectrum. The amplitude of  $B$  also traces density fluctuation level, as can be inferred from the top 2 panels of Fig. 1. At high redshifts ( $z > 50$ ) when the inhomogeneity in matter distribution is negligible,  $B$  takes unity and increases with the growth of density fluctuation. Since the collapse fraction  $f_{\text{coll}}$  indirectly reflects the density fluctuation level, this can also be seen in the left panel of Fig. 2, which shows that  $B$  grows with  $f_{\text{coll}}$ . By redshift  $z = 4$  when about 70% of matter collapsed into halos, DM annihilation rate is boosted by roughly a factor of  $10^5$  compared to the uniform background.



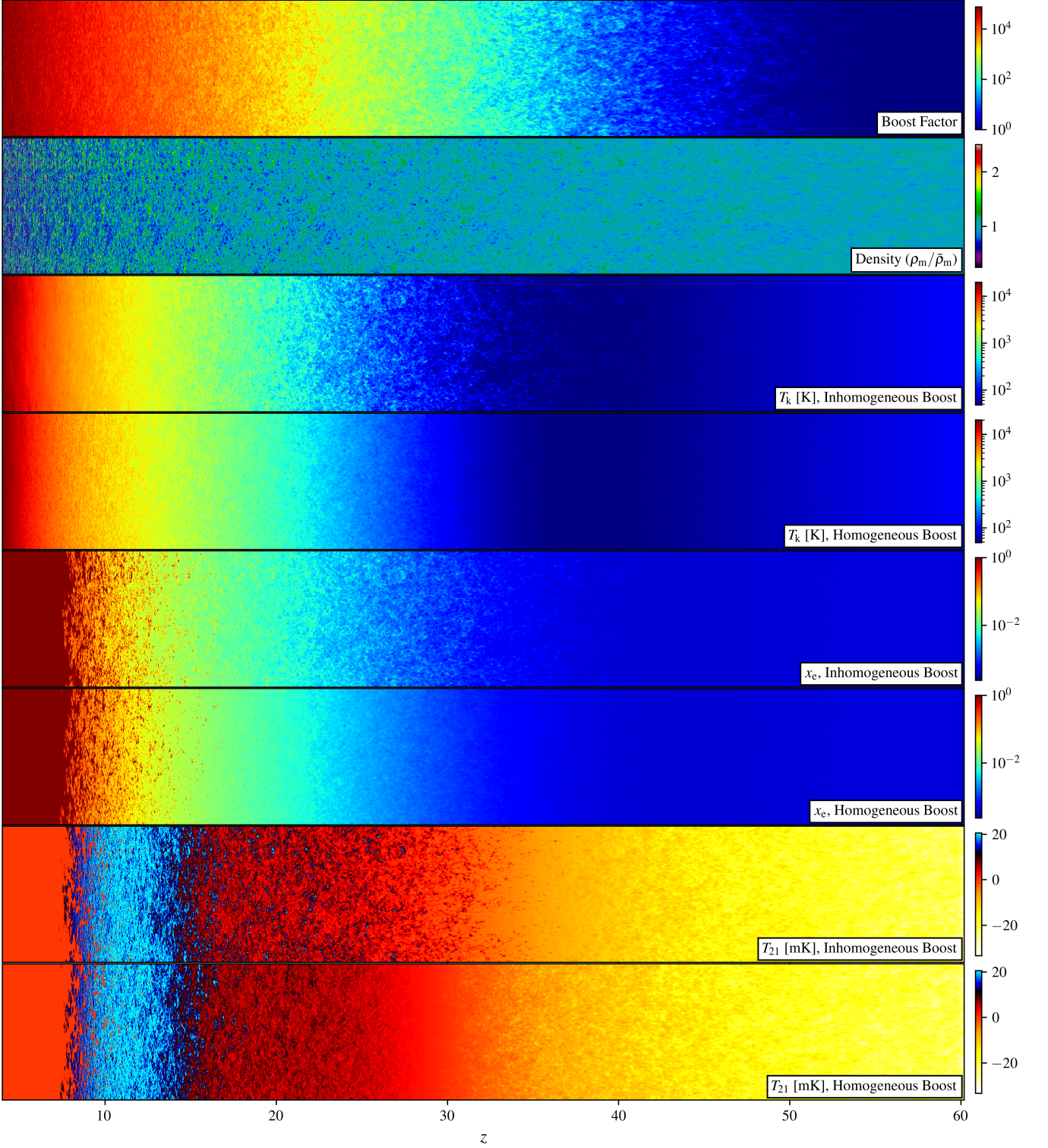


FIG. 1. Lightcone simulations of inhomogeneous boost factor (top) and the density field ( $\rho_m/\bar{\rho}_m$ ). The 2nd to 8th panels visualize the evolution of gas temperature  $T_k$ , ionisation fraction  $x_e$  and 21-cm temperature  $T_{21}$  in presence of inhomogeneous/homogeneous boost factor. Panels labeled with *Inhomogeneous Boost* corresponds to the scenario in which DM annihilation products have relatively low energy and are therefore absorbed locally. If DM injects high energy particles which has a long mean free path before absorption, the effect of inhomogeneous boost factor would be washed out. This corresponds to panels labeled with *homogeneous boost*, for which the boost factor is added uniformly using its spatially averaged value. Note that the growth and fluctuation of boost factor trace those of density field, and the panels with inhomogeneous boost factor exhibit more fluctuations than ones with homogeneous boost factor. The power spectrum shown in Fig. 3 provides more quantitative comparison of these inhomogeneities.

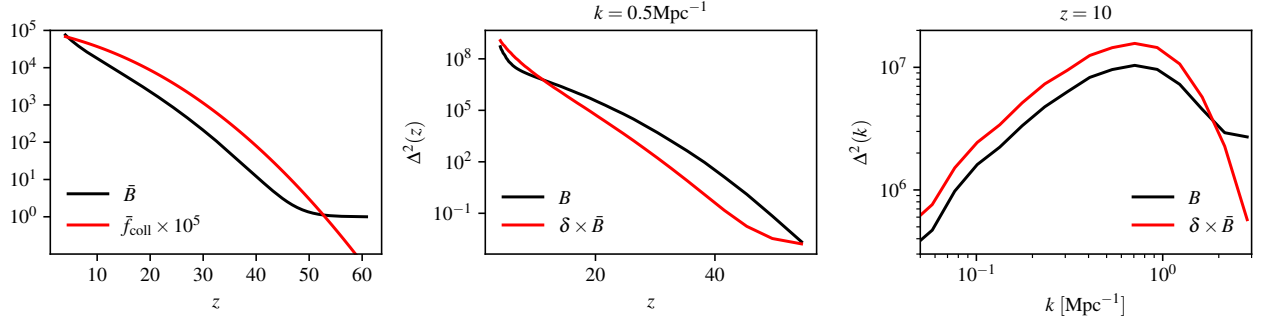


FIG. 2. *Left*—global average of boost factor  $B$  (black) and collapse fraction  $f_{\text{coll}}$  (red). *Middle and right*—power spectrum for  $B$  (black) and density contrast (red).

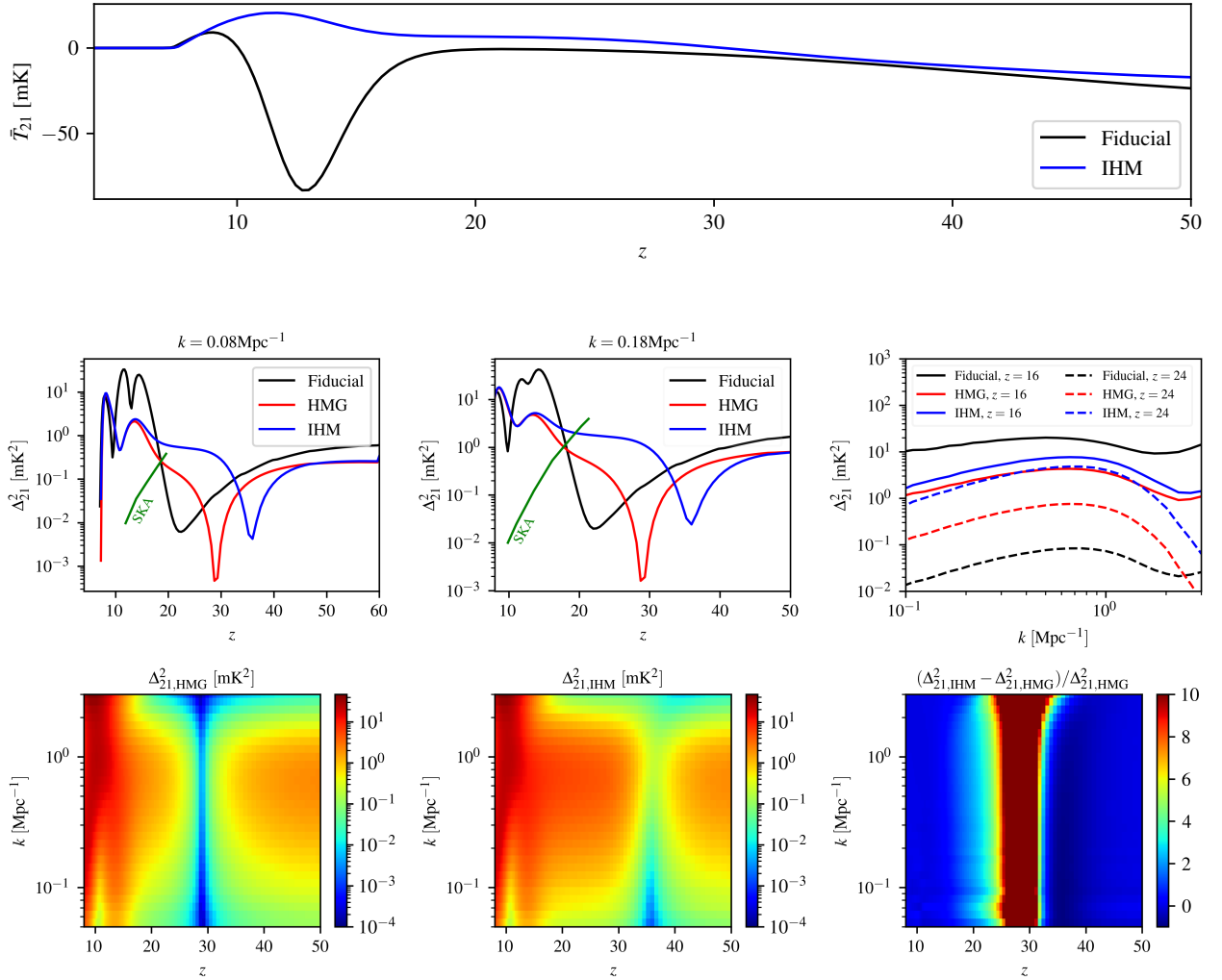


FIG. 3. *Top*: global 21-cm temperature for **Fiducial** and **IHM** simulations. Global results for the **HMG** simulation are identical to that in **IHM** scenario and are thus not shown here. Note that 21-cm absorption signal ( $T_{21} < 0$ ) is weakened or shifted into emission ( $T_{21} > 0$ ) by heating from DM. *Middle*: 21-cm power spectrum  $\Delta_{21}^2$  at several characteristic scales and redshifts. In **HMG** and **IHM** simulations  $\Delta_{21}^2$  can be enhanced by orders of magnitude. Such difference can potentially be detected by SKA telescope with 2000 hours of observation time (green solid curve) [13]. *Bottom*:  $\Delta_{21}^2$  at different scales and redshifts, the left and middle panels correspond to **HMG** and **IHM** simulations respectively. The right panel shows their relative difference. For visual illustration the color bar is truncated around 10, and note the relative difference can be much higher in some regions.

In Fig. 3 we present comparisons of global signal (top) and power spectrum (middle and lower panels) for 21-cm temperature from our simulations. We highlight the power spectrum at  $k = 0.08 \text{Mpc}^{-1}$  and  $k = 0.18 \text{Mpc}^{-1}$ , corresponding to scales which are large enough for efficient foreground removal and yet small enough for experiments to achieve high signal to noise ratio [50–53]. We also include the forecasted  $1\sigma$  power spectrum sensitivity for SKA (Square Kilometer Array) telescope computed in Refs. [13, 50], which assumed 2000 hours of observation time and an observational strategy carefully chosen to minimize thermal noise. The noise power spectrum at each  $uv$  cell was calculated in [50] as,

$$\Delta_N^2 = F \frac{k^3}{2\pi^2} T_{\text{sys}}^2 \quad (24)$$

where the factor  $F$  describes experiment beam, frequency coverage, observational strategy (see [50] for details). As we have chosen  $k$  scales that are likely free from foreground contamination, the systematic temperature  $T_{\text{sys}}$  can be expressed as the sum of sky temperature  $T_{\text{sky}}$  and receiver noise temperature  $T_{\text{rec}}$ , given by  $T_{\text{sky}} = 237(0.15 \text{GHz}/\nu)^{2.5} \text{K}$  and  $T_{\text{rec}} = 50 \text{K} + 0.1 T_{\text{sky}}$  respectively [54, 55], here the frequency  $\nu$  is related to redshift via  $z = 1.43 \text{GHz}/\nu - 1$ . For the experimental specifications, [50] adopted the SKA Low Phase 1 design [55], which has 866 station locations each with  $17 \times 17$  array and a frequency resolution of 1 kHz.

Compared to the IHM simulation,  $x_e$ ,  $T_k$  and  $T_{21}$  all display remarkably different inhomogeneity in the IHM simulation (see Fig. 1). For redshift window  $z \in [16, 30]$  in particular, inhomogeneity levels are significantly enhanced in IHM simulation due to fluctuations in DM heating/ionization rate. 21-cm power spectrum in Fig. 3 provides quantitative comparisons of these fluctuations. In presence of heating from DM, the 21-cm absorption signal ( $T_{21} < 0$ ) in the Fiducial setting is weakened or shifted into emission ( $T_{21} > 0$ ). For the HMG simulation, the change in  $\Delta_{21}^2$  relative to the Fiducial setting is largely driven by the difference in 21-cm amplitude, and we found that our global and power spectrum 21-cm signals are similar to that in [44]. However for the IHM scenario,  $\Delta_{21}^2$  is also affected by spatial variation of  $T_{21}$  induced by inhomogeneous DM heating/ionization. As shown in Fig. 3, the inhomogeneity in boost factor can enhance  $\Delta_{21}^2$  by more than a factor  $10^4$  for  $16 \lesssim z \lesssim 30$ , and such enhancement is potentially detectable at the SKA telescope [13].

## V. DISCUSSIONS

Particles injected from dark matter (DM) annihilation events can heat up the intergalactic medium and change the 21-cm signal from neutral hydrogen during the cosmic dawn. At low redshifts, the growth of structures can significantly boost DM annihilation rate relative to the uniform background. This paper examines the inhomogeneity in DM annihilation boost factor and its impact on 21-cm brightness temperature power spectrum  $\Delta_{21}^2$ . Building on the 21cmFAST simulation framework and the Press-Schechter conditional halo mass function, we obtain the lightcone evolution and the power spectrum for the inhomogeneous boost factor. We showcase the effect for an annihilation rate of  $\langle \sigma v \rangle / m_\chi = 10^{-27} \text{cm}^3 \text{s}^{-1} \text{GeV}^{-1}$ , and our result shows that compared to the case with homogeneous boost factor, which approximate long propagation length for DM annihilation products, the inhomogeneous boost factor can induce distinctively different fluctuation features in 21-cm signal in the redshift window of  $16 \lesssim z \lesssim 30$ , and the corresponding 21-cm power spectrum  $\Delta_{21}^2$  can be enhanced by more than a factor of  $10^4$ . Such features can potentially be detected by the SKA (Square Kilometer Array) telescope.

Our analysis for 21-cm signal with inhomogeneous boost factor relied on a simple on-the-spot prescription for energy deposition process, which is generally a decent approximation below electroweak energy scale or if DM annihilation primarily produce electrons. If particles injected by DM annihilation have long propagation length before absorption, the effect of inhomogeneous boost factor on 21-cm signal can be weakened or washed out. A more comprehensive analysis of the energy deposition process would necessitate a detailed study of particle cascade and propagation in an inhomogeneous background, and we reserve such investigations for future work.

### Acknowledgements

We thank Andrei Mesinger, Yuxiang Qin and Steven Murray for their helpful communications. This work is supported by the National Natural Science Foundation of China (grant No. 12275278), the National Research Foundation with grant No. 150580, and the research program “New Insights into Astrophysics and Cosmology with Theoretical Models Confronting Observational Data” of the National Institute for Theoretical and Computational Sciences of South Africa.

- 
- [1] T. R. Slatyer, SciPost Phys. Lect. Notes **53**, 1 (2022), arXiv:2109.02696 [hep-ph].
  - [2] D. Hooper, PoS **TASI2018**, 010 (2019), arXiv:1812.02029 [hep-ph].
  - [3] N. Aghanim et al. (Planck), Astron. Astrophys. **641**, A6 (2020), [Erratum: Astron.Astrophys. 652, C4 (2021)],

- arXiv:1807.06209 [astro-ph.CO].
- [4] N. Padmanabhan and D. P. Finkbeiner, Phys. Rev. D **72**, 023508 (2005), arXiv:astro-ph/0503486.
- [5] T. R. Slatyer, Phys. Rev. D **87**, 123513 (2013), arXiv:1211.0283 [astro-ph.CO].
- [6] T. R. Slatyer, Phys. Rev. D **93**, 023527 (2016),



- arXiv:1506.03811 [hep-ph].
- [7] T. R. Slatyer, Phys. Rev. D **93**, 023521 (2016), arXiv:1506.03812 [astro-ph.CO].
  - [8] H. Liu, T. R. Slatyer, and J. Zavala, Phys. Rev. D **94**, 063507 (2016), arXiv:1604.02457 [astro-ph.CO].
  - [9] M. L. Ahnen et al. (MAGIC, Fermi-LAT), JCAP **02**, 039 (2016), arXiv:1601.06590 [astro-ph.HE].
  - [10] L. Bergstrom, T. Bringmann, I. Cholis, D. Hooper, and C. Weniger, Phys. Rev. Lett. **111**, 171101 (2013), arXiv:1306.3983 [astro-ph.HE].
  - [11] G. Giesen, M. Boudaud, Y. Génolini, V. Poulin, M. Cirelli, P. Salati, and P. D. Serpico, JCAP **09**, 023 (2015), arXiv:1504.04276 [astro-ph.HE].
  - [12] J. R. Pritchard and A. Loeb, Rept. Prog. Phys. **75**, 086901 (2012), arXiv:1109.6012 [astro-ph.CO].
  - [13] M. Sitwell, A. Mesinger, Y.-Z. Ma, and K. Sigurdson, Mon. Not. Roy. Astron. Soc. **438**, 2664 (2014), arXiv:1310.0029 [astro-ph.CO].
  - [14] A. Mesinger, S. Furlanetto, and R. Cen, Mon. Not. Roy. Astron. Soc. **411**, 955 (2011), arXiv:1003.3878 [astro-ph.CO].
  - [15] S. Furlanetto, S. P. Oh, and F. Briggs, Phys. Rept. **433**, 181 (2006), arXiv:astro-ph/0608032.
  - [16] S. G. Murray, The Journal of Open Source Software **3**, 850 (2018), arXiv:1809.05030 [astro-ph.IM].
  - [17] J. Park, A. Mesinger, B. Greig, and N. Gillet, Mon. Not. Roy. Astron. Soc. **484**, 933 (2019), arXiv:1809.08995 [astro-ph.GA].
  - [18] R. J. Bouwens et al., Astrophys. J. **803**, 34 (2015), arXiv:1403.4295 [astro-ph.CO].
  - [19] R. J. Bouwens, G. D. Illingworth, P. A. Oesch, J. Caruana, B. Holwerda, R. Smit, and S. Wilkins, Astrophys. J. **811**, 140 (2015), arXiv:1503.08228 [astro-ph.CO].
  - [20] P. A. Oesch, R. J. Bouwens, G. D. Illingworth, I. Labbé, and M. Stefanon, The Astrophysical Journal **855**, 105 (2018).
  - [21] R. Adam et al. (Planck), Astron. Astrophys. **596**, A108 (2016), arXiv:1605.03507 [astro-ph.CO].
  - [22] I. McGreer, A. Mesinger, and V. D’Odorico, Mon. Not. Roy. Astron. Soc. **447**, 499 (2015), arXiv:1411.5375 [astro-ph.CO].
  - [23] F. Ziparo, S. Gallerani, A. Ferrara, and F. Vito, Mon. Not. Roy. Astron. Soc. **517**, 1086 (2022), arXiv:2209.09907 [astro-ph.CO].
  - [24] J. F. Navarro, C. S. Frenk, and S. D. M. White, Astrophys. J. **490**, 493 (1997), arXiv:astro-ph/9611107.
  - [25] R. Barkana and A. Loeb, Phys. Rept. **349**, 125 (2001), arXiv:astro-ph/0010468.
  - [26] C. G. Lacey and S. Cole, Mon. Not. Roy. Astron. Soc. **262**, 627 (1993).
  - [27] R. S. Somerville and T. S. Kolatt, Mon. Not. Roy. Astron. Soc. **305**, 1 (1999), arXiv:astro-ph/9711080.
  - [28] A. Cooray and R. K. Sheth, Phys. Rept. **372**, 1 (2002), arXiv:astro-ph/0206508.
  - [29] J. E. Taylor and J. Silk, Mon. Not. Roy. Astron. Soc. **339**, 505 (2003), arXiv:astro-ph/0207299.
  - [30] G. Huetsi, A. Hektor, and M. Raidal, Astron. Astrophys. **505**, 999 (2009), arXiv:0906.4550 [astro-ph.CO].
  - [31] J. Cang, Y. Gao, and Y.-Z. Ma, JCAP **03**, 012 (2022), arXiv:2108.13256 [astro-ph.CO].
  - [32] T. R. Slatyer, N. Padmanabhan, and D. P. Finkbeiner, Phys. Rev. D **80**, 043526 (2009), arXiv:0906.1197 [astro-ph.CO].
  - [33] H. Liu, G. W. Ridgway, and T. R. Slatyer, Phys. Rev. D **101**, 023530 (2020), arXiv:1904.09296 [astro-ph.CO].
  - [34] Y. Sun, J. W. Foster, H. Liu, J. B. Muñoz, and T. R. Slatyer, (2023), arXiv:2312.11608 [hep-ph].
  - [35] X.-L. Chen and M. Kamionkowski, Phys. Rev. D **70**, 043502 (2004), arXiv:astro-ph/0310473.
  - [36] J. M. Shull and M. E. van Steenberg, Astrophys. J. **298**, 268 (1985).
  - [37] S. Galli, T. R. Slatyer, M. Valdes, and F. Iocco, Phys. Rev. D **88**, 063502 (2013), arXiv:1306.0563 [astro-ph.CO].
  - [38] S. Furlanetto and S. J. Stoeve, Mon. Not. Roy. Astron. Soc. **404**, 1869 (2010), arXiv:0910.4410 [astro-ph.CO].
  - [39] M. Valdes, C. Evoli, and A. Ferrara, Mon. Not. Roy. Astron. Soc. **404**, 1569 (2010), arXiv:0911.1125 [astro-ph.CO].
  - [40] C. Evoli, M. Valdes, A. Ferrara, and N. Yoshida, Mon. Not. Roy. Astron. Soc. **422**, 420 (2012).
  - [41] Y. Ali-Haïmoud and C. M. Hirata, Phys. Rev. D **83**, 043513 (2011), arXiv:1011.3758 [astro-ph.CO].
  - [42] N. Lee and Y. Ali-Haïmoud, Phys. Rev. D **102**, 083517 (2020), arXiv:2007.14114 [astro-ph.CO].
  - [43] J. B. Muñoz, Y. Qin, A. Mesinger, S. G. Murray, B. Greig, and C. Mason, Mon. Not. Roy. Astron. Soc. **511**, 3657 (2022), arXiv:2110.13919 [astro-ph.CO].
  - [44] L. Lopez-Honorez, O. Mena, A. Moliné, S. Palomares-Ruiz, and A. C. Vincent, JCAP **08**, 004 (2016), arXiv:1603.06795 [astro-ph.CO].
  - [45] K. Short, J. L. Bernal, A. Raccanelli, L. Verde, and J. Chluba, JCAP **07**, 020 (2020), arXiv:1912.07409 [astro-ph.CO].
  - [46] V. Poulin, P. D. Serpico, and J. Lesgourgues, JCAP **12**, 041 (2015), arXiv:1508.01370 [astro-ph.CO].
  - [47] R. Diamanti, L. Lopez-Honorez, O. Mena, S. Palomares-Ruiz, and A. C. Vincent, JCAP **02**, 017 (2014), arXiv:1308.2578 [astro-ph.CO].
  - [48] A. Natarajan and D. J. Schwarz, Phys. Rev. D **81**, 123510 (2010), arXiv:1002.4405 [astro-ph.CO].
  - [49] M. Valdes, C. Evoli, A. Mesinger, A. Ferrara, and N. Yoshida, Mon. Not. Roy. Astron. Soc. **429**, 1705 (2013), arXiv:1209.2120 [astro-ph.CO].
  - [50] A. Mesinger, A. Ewall-Wice, and J. Hewitt, Mon. Not. Roy. Astron. Soc. **439**, 3262 (2014), arXiv:1310.0465 [astro-ph.CO].
  - [51] A. Lidz, O. Zahn, M. McQuinn, M. Zaldarriaga, and L. Hernquist, Astrophys. J. **680**, 962 (2008), arXiv:0711.4373 [astro-ph].
  - [52] J. S. Dillon et al., Phys. Rev. D **89**, 023002 (2014), arXiv:1304.4229 [astro-ph.CO].
  - [53] J. C. Pober et al., Astrophys. J. Lett. **768**, L36 (2013), arXiv:1301.7099 [astro-ph.CO].
  - [54] A. E. E. Rogers and J. D. Bowman, Astron. J. **136**, 641 (2008), arXiv:0806.2868 [astro-ph].
  - [55] P. E. Dewdney et al., “Skal system baseline design,” [http://www.caastro.org/files/0/1503117833/ska-tel-sko-dd-001-1\\_baselinedesign1.pdf](http://www.caastro.org/files/0/1503117833/ska-tel-sko-dd-001-1_baselinedesign1.pdf) (2013).